

Computational, Spectral and Structural Studies of New Hydrazinium Hydrogen Phthalate Monohydrate Salt

L. RAJASEKAR[✉], T.M. AHAMED HUSSAIN[✉] and B.N. SIVASANKAR^{*✉}

Department of Chemistry, Government Arts College, Udhamandalam, The Nilgiris-643002, India

*Corresponding author: E-mail: sivabickol@yahoo.com

Received: 4 April 2022;

Accepted: 31 May 2022;

Published online: 18 July 2022;

AJC-20899

Pure single crystals of Lewis acid-base salt, hydrazinium hydrogen phthalate monohydrate (HHPMH) has been synthesized, crystallized and isolated as a single crystal by slow evaporation method at room temperature (22 °C). Analysis of analytical, spectral, thermal and structural data confirmed the salt formation in aqueous medium. The analytical data is in favour of the proposed composition $\text{HOOC-C}_6\text{H}_4\text{COO N}_2\text{H}_5 \cdot \text{H}_2\text{O}$. The compound crystallized in a monoclinic crystal system and $P2_1/c$ space group with cell parameters, $a = 15.409(3)$ Å, $b = 10.292(2)$ Å and $c = 6.7087(12)$ Å. Though strong intramolecular hydrogen bonding interaction is anticipated between acidic hydrogen of HHPMH and deprotonated carboxylate oxygen surprisingly in the present case it is absent and a weak interaction is observed between acidic hydrogen and water molecule, which is quite evident from the ORTEP diagram. The nature of interactions between hydrazine cation and hydrogen phthalate ion and the crystal packing diagram from various types of intermolecular contacts were determined by Hirshfeld surface analysis. The compound was stable up to 40 °C and undergoes dehydration from 40-70 °C with an endotherm at 47 °C. The experimental and theoretical infrared spectra are also in favour of the formation of ionic crystal. The molecular structure was optimized using B3LYP method by 6-311G (d,p) basis set. The energy gap between HOMO and LUMO is 7.7340 eV. Theoretical calculation based on DFT studies and natural bond orbital analyses has been carried out to evaluate the molecular electrostatic potential. The structure was optimized by DFT and the vibrational frequencies were calculated. Comparison of experimental and optimized structures revealed that there is a good coincidence between the two.

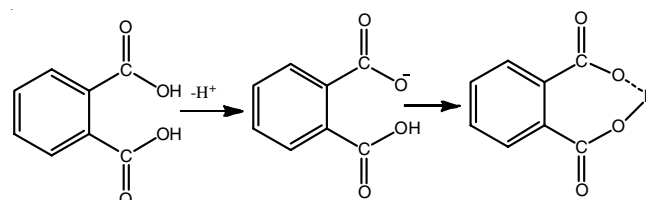
Keywords: Lewis acid, Hydrazinium hydrogenphthalate, Single crystal, Hirshfeld surface analysis.

INTRODUCTION

Recent advances in the optical technologies prompt researchers to develop new materials for non-linear application [1-7]. Organic crystalline materials with hydrogen bonding interaction, delocalized electrons and high dipole moments are the requirements for excellent NLO properties [8-12]. Interesting structural features of the organic ionic crystals are observed with compounds having the ability of protonation and hydrogen bond formation [13-15]. Interesting properties like dipole moment, hyperpolarizability, mulliken charges, molecular electrostatic potential, HOMO-LUMO energy gap, etc. depend on the structural features of the crystals. The relation between geometry and microscopic properties can be well investigated by quantum mechanical and chemical calculations.

Benzene 1,2-dicarboxylic acid, phthalic acid is an aromatic dicarboxylic acid with two acidic protons with pK_a values 2.89

and 5.51. One proton with lower pK_a value can be replaced by even weak bases like ammonia, hydrazine and its derivatives. However, the second proton could not replace with these weak bases because of the intramolecular hydrogen bonding interaction as shown below:



Hence, weak bases in aqueous medium yield mono salts and strong bases give both mono and disalts. The resulting salts gain great attention in non-linear optical research because of the active participation of intermolecular and intramolecular

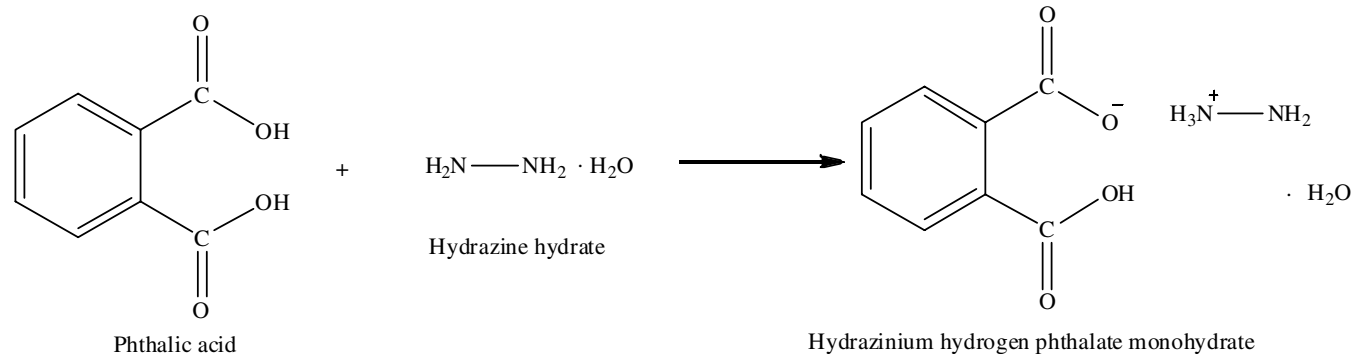
hydrogen bonding and molecular hyperpolarizability which lead to optical response. The combination of hydrazine with phthalic acid would lead to the crystal of improved optical nonlinearity. Hence, the present research has been carried out for the first time to synthesize and investigate the structure of hydrazinium phthalate as a single crystal. Theoretical calculation based on DFT and Hirshfeld analyses were carried out to investigate the molecular electrostatic potential, HOMO-LUMO energy gap, vibrational spectra, NBO, first-order hyperpolarizability of the title compound.

Hydrazine is a versatile compound which has the ability to react both in aqueous and organic media so that both ionic salts and condensation compounds could be isolated from this diamine. Due to its weak basic nature, it forms crystalline salts with mineral as well as carboxylic acids. Though it is a diacidic base, formation of monohydrazine salts has been reported in the literature except for a few hydrazonium salts [16,17]. Furthermore, this compound deprotonates hydrogen from organic acids with lower pK_a values. The hydrazine salts are usually crystalline, hydrated and stabilized by hydrogen bonding interaction and van der Waals forces.

Hydrazine is the simplest diamine and diacidic weak base which is weaker than ammonia. In aqueous medium when treated with acids, hydrazine forms monohydrazinium ($N_2H_5^+$), dihydrazinium ($N_2H_5^+$)₂ or hydrazonium ($N_2H_6^{2+}$) (strong acids) salts. Several salts of hydrazine and its derivatives have been reported in the literature and their properties have been investigated [18]. Though hydrazine phthalate has been reported from our laboratory, its structure and detailed theoretical studies have not been attempted so far [19]. Hence, in this article, we wish to report the synthesis and structural and DFT investigation on hydrazinium hydrogen phthalate monohydrate single crystal.

EXPERIMENTAL

Synthesis of hydrazinium hydrogen phthalate monohydrate (HHPMH): Hydrazine hydrate monohydrate (5 mL, 0.1 mol) and phthalic acid (1.64 g, 0.1 mol) were separately dissolved in 30 mL each of distilled water and the base was added to phthalic acid slowly with constant stirring. The mixture was filtered and kept aside at room temperature for about two weeks in a dust-free atmosphere at 24 °C. Pure HHPMH crystals were removed after 15 days, washed with ice-cold distilled water and dried in air (**Scheme-I**). Yield: 54%; calcd. (found) %: C, 44.40 (44.35); H, 4.99 (4.86); N₂H₄, 14.76 (14.50).



Scheme-I: Synthetic route of hydrazinium hydrogen phthalate monohydrate

Computational details: All the solvents and chemicals were procured from S.D. Fine Chemicals, India. Under Andrew's condition [20], hydrazine concentration was estimated by conducting volumetric analyses by using a 0.025 M KIO₃ solution. Elemental analyses (CHN) were performed using the Perkin-Elmer 2400 CHN elemental analyser. The IR spectrum of the salt was recorded (KBr disc) in 4000-400 cm⁻¹ on the Bruker alpha spectrophotometer. The TG-DTA of the sample was simultaneously measured in air with the SWI TG/DTA 6200 thermal analyser by using a platinum cup as the sample holder and approximately 5 mg of sample at the heating rate of 10 °C/min. The data of X-ray single crystal intensity were obtained using the Enraf-Nonius CAD-4 diffractometer system having graphite monochromated MoK α radiation ($\lambda = 0.71073$ Å). The salt structure was determined using the direct method by employing the completed using Fourier techniques and SIR 92 program and was refined by applying full-matrix least square method. Refinement was performed using SHELXL-2014 program [21,22]. With CRYSTALEXPLORER 17.1 program, Hirshfeld surface calculations were conducted [23]. Parameters, such as natural bond orbital (NBO) analysis, molecular geometry optimisation, hyperpolarizability and molecular electrostatic potential (MEP) were calculated using the B3LYP method by employing the 6-311+G(d,p) level of theory with Gaussian 16 software package [24].

RESULTS AND DISCUSSION

Hydrazine hydrate in an aqueous medium reacts with phthalic acid in a 1:1 molar ratio to yield hydrazinium hydrogen phthalate monohydrate. Present attempts to isolate dihydrazinium phthalate and hydrazonium phthalate by reacting hydrazine hydrate and phthalic acid in 2:1 and 1:2 ratio, respectively were not successful. It could be due to the higher pK_a value of the second proton of phthalic acid and instability of hydrazonium salt, respectively. Formation of hydrazinium hydrogen phthalate monohydrate (HHPMH) has been confirmed by identification and determination of hydrazine in the single crystal of the salt and also by spectral and thermal studies.

Infrared spectrum: Usually, carboxylic acids form either salts or molecular adducts when reacting with Lewis bases. In present case, formation of salt has been confirmed by the vibrational spectrum. The asymmetric and symmetric carboxylate stretchings of phthalic acid are observed in the region 1650 and 1560 cm⁻¹, respectively. The HHPMH salt shows these bands

in the region 1580 and 1420 cm^{-1} . The decrease in asymmetric stretching in the salt favour the abstraction of a highly acidic proton ($\text{p}K_a = 2.89$) by $-\text{NH}_2$ group in hydrazine and also due to the intramolecular hydrogen bonding. The expected asymmetric stretching of the free COOH group of HHPMH is not in the same region 1720 cm^{-1} which is observed in the case of phthalic acid indicating the intramolecular hydrogen bonding interaction. Though intramolecular hydrogen bonding is expected between the carboxylic acid hydrogen and other neutral atoms of HHPMH as carboxylic acid of HHPMH, the decreases in carbonyl asymmetric stretching of this moiety of salt is very small which is not very much in favour of this interaction. Hence, the O-H stretching and N-H stretchings of the salt absorbed as a broad band in the region 3500-3400 cm^{-1} .

However, broad bands from 3400 extending up to 2600 cm^{-1} are attributed to the weak intermolecular hydrogen bond in this compound though it is not very clear at this stage. From the foregoing discussions, it is very clear that the free carboxylic acid hydrogen, in this case, is not bound to the *ortho* carboxylate group, which is expected to be very strong and in turn expected to decrease the carbonyl stretching frequency of the free carboxylic acid. Hence, the hydrogen bonding interactions are proposed for the salt concerning the carboxylic acid. The infrared spectrum of the salt is shown in Fig. 1.

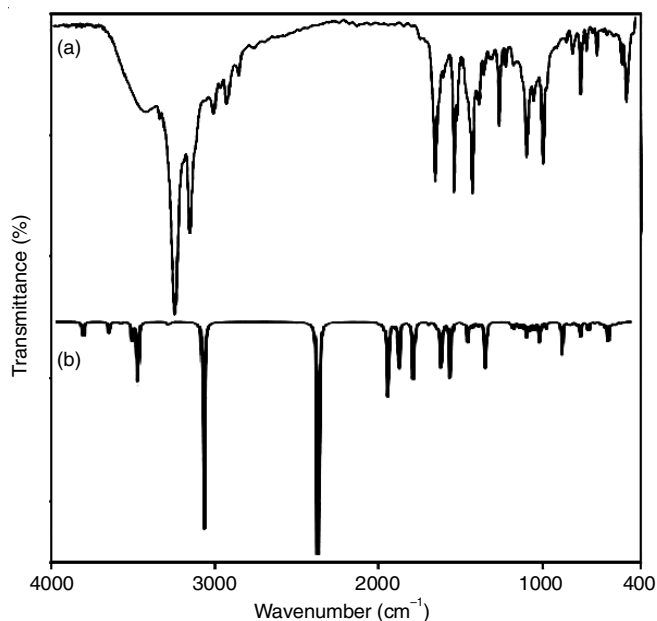


Fig. 1. (a) Experimental FT-IR spectrum (b) Theoretical FT-IR spectrum of HHPMH

Crystal structure description: The hydrazinium hydrogen phthalate monohydrate crystallizes in a monoclinic crystal system with a $P2_1/c$ space group. The unit cell parameters are $a = 15.409(3)$ Å, $b = 10.292(2)$ Å and $c = 6.7087(12)$ Å. The crystal density determined is 1.385 mg/m^3 which is very close to that calculated value (1.380 mg/m^3) from X-ray crystal data. There are four molecules present in a unit cell, which are connected by hydrogen bonding interactions and weak van der Waals forces. The crystal data and structural refinement data are given in Table-1. The ORTEP (50% probability

TABLE-1
CRYSTAL DATA AND STRUCTURE REFINEMENT OF HHPMH

CCDC No	1477688
Empirical formula	$\text{C}_8\text{H}_{12}\text{N}_2\text{O}_5$
Formula weight	216.20
Temperature	293(2) K
Wavelength	0.71073 Å
Crystal system	Monoclinic
Space group	$P2_1/c$
Unit cell dimensions	$a = 15.409(3)$ Å, $\alpha = 90^\circ$ $b = 10.292(2)$ Å, $\beta = 101.942(7)^\circ$ $c = 6.7087(12)$ Å, $\gamma = 90^\circ$
Volume	1040.9(3) Å ³
Z	4
Density (calculated)	1.380 Mg/m^3
Absorption coefficient	0.116 mm^{-1}
F(000)	456
Crystal size	0.350 × 0.250 × 0.200 mm^3
Theta range for data collection	2.396 to 25.000°
Index ranges	-18 ≤ h ≤ 18, -12 ≤ k ≤ 12, -7 ≤ l ≤ 7
Reflections collected	11789
Independent reflections	11789 [R(int) = ?]
Completeness to theta = 25.000°	99.5 %
Absorption correction	Semi-empirical from equivalents
Max. and min. transmission	0.96 and 0.93
Refinement method	Full-matrix least-squares on F^2
Data/restraints/parameters	11789/6/159
Goodness-of-fit on F^2	1.059
Final R indices [I > 2σ(I)]	R1 = 0.0552, wR2 = 0.1089
R indices (all data)	R1 = 0.0929, wR2 = 0.1293
Extinction coefficient	0.006(2)
Largest diff. peak and hole	0.295 and -0.263 e.Å^{-3}

ellipsoid) representation of the molecule with the atom numbering scheme is shown in Fig. 2. Hydrazinium hydrogen phthalate monohydrate single crystal consists of discrete hydrazinium cation, hydrogen phthalate anion and one water molecule. The N_2H_5^+ ions connected to the carboxylate groups of phthalate ion by weak hydrogen bonding interaction. Hydrazinium cation is surrounded by six oxygen atoms through the hydrogen atom of hydrazine. The $\text{C}_1\text{-O}_2$ bond distance *i.e.* carbonyl bond length of free carboxylic acid is 1.217 Å, which is the shortest among the C-O bond and C-OH bond. The hydrogen bonding (Fig. 3) clearly shows that the acidic hydrogen of HHPA is weakly interacted with the water oxygen and does not have any interaction with the carboxylate oxygen atoms. In the present case, complete hydrogen transfer taking place from phthalic acid to hydrazine molecule.

Thermal analysis: Thermal analysis of HHPMH crystal was studied and its TG-DTA traces are shown in Fig. 4. In the TG curve initially, there is an 8% weight loss in the temperature range 40-70 °C is due to the elimination of lattice water, which confirms the hydrated nature of the title crystal. The calculated weight loss is 8.32%. Dehydration is associated with an endotherm at 52 °C in the DTA curve. Another endotherm at 190 °C with a TG weight loss of 14% (calcd. 14.81%) in the second stage is attributed to the dehydrazination to yield phthalic acid as an intermediate. The successive thermal event observed between 200-350 °C with an endotherm at 340 °C shows the complete decomposition of HHPMH and its residues.

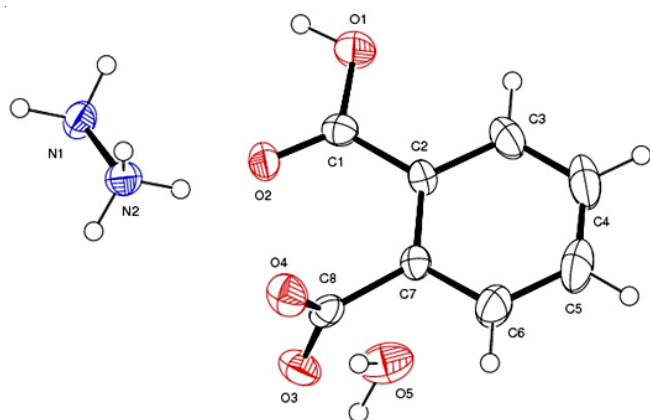


Fig. 2. ORTEP of HHPMH at 50% probability

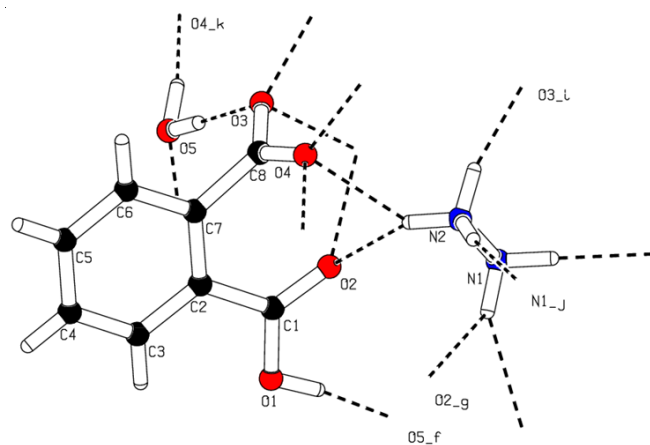


Fig. 3. Hydrogen bonding diagram in HHPMH

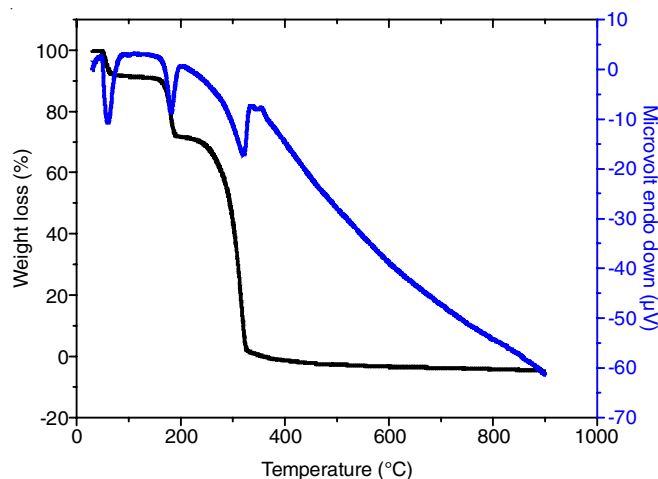


Fig. 4. Simultaneous TG-DTA plots of HHPMH

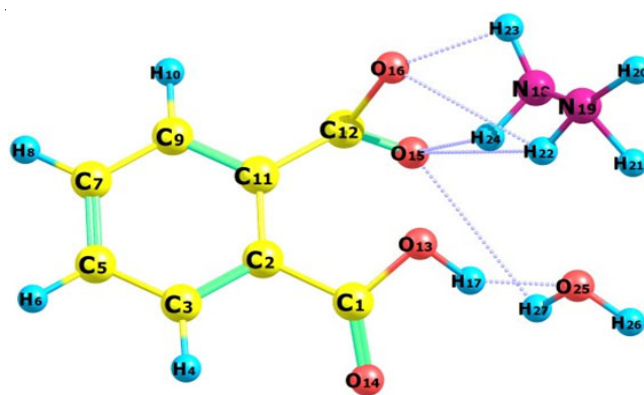


Fig. 5. Optimized geometry of HHPMH

Optimized geometry: Optimized geometry parameters of the salt were calculated by DFT (B3LYP functional) using B3LYP/6-311G+ (d,p) basis set and the optimized molecular geometry of HHPMH is shown in Fig. 5. The calculated bond lengths and bond angles of the B3LYP/6-311G+ (d,p) basis set are in good agreement with the experimental values which are listed in Tables 2 and 3, respectively.

Those results are supported by statistical analysis based on the linear regression method (r^2) for structural geometrical parameters. The electronic energy of the B3LYP/6-311G+ (d,p)

basis set shows -2371.53 Hartree, which is minimum compared to all other levels of basis sets.

The hydrogen phthalate molecule is linked to other molecules/ions through various intermolecular interactions which are shown in Table-4. They are $N_2-H_{2A}-O_2$, $N_2-H_{2A}-O_4$, $N_2-H_{2B}-O_3$, $N_2-H_{2C}-N_1$, $O_1-H_1-O_5$, $N_1-H_{1A}-O_2$, $N_1-H_{1A}-O_3$, $N_1-H_{1B}-O_4$, $O_5-H_{5A}-O_4$ and $O_5-H_{5B}-O_3$ with hydrogen bond lengths 2.21, 2.26, 1.85, 2.04, 1.65, 2.34, 2.32, 1.96, 1.86 and 1.89 Å, respectively. These strong intermolecular hydrogen bonding interactions increase the stability of the molecule.

TABLE-2
EXPERIMENTAL AND CALCULATED BOND LENGTH VALUES OF HHPMH

Atoms	SXRD bond length values (Å)	Calculated bond length values (Å) B3LYP/6-311G+ (d,p)	Atoms	SXRD bond length values (Å)	Calculated bond length values (Å) B3LYP/6-311G+ (d,p)
C(1)-O(2)	1.217	1.237	C(7)-C(8)	1.508	1.489
C(1)-O(1)	1.315	1.362	C(8)-O(3)	1.253	1.248
C(1)-C(2)	1.480	1.492	C(8)-O(4)	1.254	1.347
C(2)-C(3)	1.389	1.397	N(1)-N(2)	1.447	1.460
C(2)-C(7)	1.395	1.412	N(1)-H(1A)	0.90	1.031
C(3)-C(4)	1.378	1.398	N(1)-H(1B)	0.95	1.019
C(3)-H(3)	0.930	1.081	N(2)-H(2A)	0.890	1.016
C(4)-C(5)	1.369	1.392	N(2)-H(2B)	0.890	1.018
C(4)-H(4)	0.930	1.082	N(2)-H(2C)	0.890	1.016
C(5)-C(6)	1.375	1.398	O(1)-H(1)	0.92	1.011
C(5)-H(5)	0.930	1.082	O(5)-H(5A)	0.93	0.99
C(6)-C(7)	1.383	1.396	O(5)-H(5B)	0.87	0.97
C(6)-H(6)	0.930	1.081			

TABLE-3
EXPERIMENTAL AND CALCULATED BOND ANGLE VALUES OF HHPMH

Atoms	SXRD bond angles (°)	Calculated bond angles (°) B3LYP/6-311G+ (d,p)	Atoms	SXRD bond angles (°)	Calculated bond angles (°) B3LYP/6-311G+ (d,p)
O(2)-C(1)-O(1)	122.6	124.2	C(7)-C(6)-H(6)	119.8	120.5
O(2)-C(1)-C(2)	122.8	124.8	C(6)-C(7)-C(2)	119.2	119.9
O(1)-C(1)-C(2)	114.6	110.9	C(6)-C(7)-C(8)	117.3	119.3
C(3)-C(2)-C(7)	119.5	119.6	C(2)-C(7)-C(8)	123.5	119.6
C(3)-C(2)-C(1)	120.3	120.01	O(3)-C(8)-O(4)	124.4	124.0
C(7)-C(2)-C(1)	120.1	120.3	O(3)-C(8)-C(7)	118.8	123.8
C(4)-C(3)-C(2)	120.6	120.2	O(4)-C(8)-C(7)	116.7	112.2
C(4)-C(3)-H(3)	119.7	120.8	N(2)-N(1)-H(1A)	108.0	111.3
C(2)-C(3)-H(3)	119.7	118.9	N(2)-N(1)-H(1B)	108.0	111.3
C(5)-C(4)-C(3)	119.5	120.0	H(1A)-N(1)-H(1B)	103.0	105.7
C(5)-C(4)-H(4)	120.3	120.1	N(1)-N(2)-H(2A)	109.5	109.6
C(3)-C(4)-H(4)	120.3	120.1	N(1)-N(2)-H(2B)	109.5	110.3
C(4)-C(5)-C(6)	120.9	120.1	H(2A)-N(2)-H(2B)	109.5	111.4
C(4)-C(5)-H(5)	119.5	119.7	N(1)-N(2)-H(2C)	109.5	109.7
C(6)-C(5)-H(5)	119.5	120.6	H(2A)-N(2)-H(2C)	109.5	110.4
C(5)-C(6)-C(7)	120.3	120.0	H(2B)-N(2)-H(2C)	109.5	110.1
C(5)-C(6)-H(6)	119.8	119.3	C(1)-O(1)-H(1)	109.5	115.1
			H(5A)-O(5)-H(5B)	100.0	113.8

TABLE-4
HYDROGEN BONDING INTERACTION OF HHPMH

D-H...A	d(D-H)	d(H...A)	d(D...A)	∠(DHA)
N(2)-H(2A)...O(2)	0.89	2.21	2.921(5)	136.2
N(2)-H(2A)...O(4)	0.89	2.26	2.963(6)	135.7
N(2)-H(2B)...O(3)#1	0.89	1.85	2.714(6)	164.1
N(2)-H(2C)...N(1)#2	0.89	2.04	2.927(6)	171.5
O(1)-H(1)...O(5)#2	0.92(5)	1.65(5)	2.565(5)	172(5)
N(1)-H(1A)...O(2)#2	0.90(4)	2.34(5)	3.039(7)	134(5)
N(1)-H(1A)...O(3)#2	0.90(4)	2.37(5)	3.136(6)	143(5)
N(1)-H(1B)...O(4)#3	0.95(4)	1.96(4)	2.904(6)	176(6)
O(5)-H(5A)...O(4)#4	0.93(4)	1.86(4)	2.769(7)	167(7)
O(5)-H(5B)...O(3)	0.87(4)	1.89(4)	2.759(7)	179(6)

Symmetry transformations used to generate equivalent atoms:

#1-x+2,-y,-z+1; #2 x,-y-1/2,z+1/2; #3-x+2,y-1/2,-z+3/2; #4 x,y,z-1

In hydrogen phthalate anion, C₁-O₂, C₁-O₁, C₈-O₃ and C₈-O₄ bond lengths are 1.237, 1.362, 1.248 and 1.347 Å, respectively which are in good agreement with the experimental values of 1.217, 1.315, 1.253 and 1.254 Å, respectively. The N-N bond length calculated theoretically is 1.460 Å, is close to the experimental value of 1.447 Å. The experimental and theoretical bond lengths and bond angles are compared and summarized in Tables 2 and 3, respectively. The optimized structure and their geometrical parameters are in good agreement with the single-crystal X-ray diffraction results.

Natural bond orbital (NBO) analysis: The NBO analysis is efficient for studying the intermolecular and intramolecular interactions that occur in a molecular system and serves as a convenient tool for investigating conjugative interaction or charge transfer in the molecular system. At the B3LYP/6-311+G(d, p) level, the second-order perturbation theory was utilized to estimate donor-acceptor interactions by employing Gaussian 16 software with NBO 6.1 program.

The NBO study indicated that the HHPMH molecule formed through the strong interactions N-H...N and N-H...O hydrogen bonding between the σ^* (N-H) antibonding orbitals and lone pairs of oxygen atoms. Table-5 presents different

hyperconjugative interactions that occur in HHPMH. These hyperconjugative interactions of donor-acceptor led to the delocalization of the electron within the system; this delocalization facilitates charge transfer within the molecule and was mediated through intermolecular hydrogen bonding. According to the NBO analysis of HHPMH, strong intermolecular H-bonds were formed among the water oxygen, carboxylate oxygen and N-H groups of a cationic moiety. Different hyperconjugative interactions, including LP(2) O2 → σ^* (N2-H7) (13.44 kcal/mol), LP(1) O3 → σ^* (O5-H11) (7.35 kcal/mol), LP(1) N2 → π^* (O2-C1) (1.15 kcal/mol), and LP(1) N1 → π^* (O5-H11) (1.13 kcal/mol), were associated with the stabilization energy E(z) presented in Table-5 and employed to quantify the extent of intermolecular hydrogen bonding of carboxylate oxygen and water with N-H. In the aromatic ring, the hyperconjugative interactions of π^* (C4-C5) → π^* (C6-C7) and π^* (C4-C5) → π^* (C2-C3) exhibited high stabilization energy of 150.45 and 120.34 kcal/mol, respectively. The NBO study revealed that the hyperconjugative interactions of σ (C-C) → σ^* (C-C) and π (C-C) → π^* (C-C) occurred within the benzene ring. In HHPMH, among these two interactions, π (C-C) → π^* (C-C) conjugation was dominant and led to charge transfer within HHPMH and resonance within the benzene ring.

Mulliken charge analysis: Fig. 6 presents the plots of the Mulliken charge distribution on different HHPAM atoms. Mulliken atomic charges were calculated using the B3LYP/6-311G+(d,p) basis set. All nitrogen and oxygen atoms carry a negative charge. These negative charges serve as electron donors. Among oxygen atoms, O25 (-0.9067 e) shows a higher negative charge than O16 (-0.5527 e), O15 (-0.3889 e) and O13 (-0.3941 e) because of hydrogen bonding. With electron delocalization, the amino nitrogen N19 (-0.9504) and N18 (-0.3561 e) become negatively charged. Each hydrogen atom of the molecule exhibits a positive charge, particularly H21 (0.5421 e), H27 (0.4504 e) and H17 (0.4194 e) exhibit the highest charge value because of their involvement in hydrogen

TABLE-5
SECOND ORDER PERTURBATION THEORY
ANALYSIS OF FOCK MATRIX IN NBO BASIS

Donor	Occu- pancy	Acceptor	Occu- pancy	E (2) (Kcal/mol)
$\sigma(O3-C8)$	1.59	$\sigma^*(O4-C8)$	0.75	1.76
$\sigma(O3-C8)$	1.45	$\sigma^*(C7-C8)$	0.94	2.18
LP (1)O 3	1.73	$\sigma^*(O5-H11)$	0.08	3.76
LP (2)O 3	0.69	$\sigma^*(O5-H11)$	0.08	1.34
LP (1)N 1	1.75	$\sigma^*(O5-H11)$	0.08	1.13
LP(1)N 2	1.81	$\pi^*(O2-C1)$	0.33	1.15
$\sigma(C2-C3)$	1.78	$\sigma^*(C3-C4)$	0.04	2.82
$\sigma(C2-C3)$	1.75	$\sigma^*(C5-C6)$	0.05	4.67
$\pi(C2-C3)$	0.65	$\pi^*(C4-C5)$	0.28	2.44
$\pi(C2-C3)$	0.58	$\pi^*(C6-C7)$	0.28	3.87
$\sigma(C4-C5)$	1.79	$\sigma^*(C1-C2)$	0.35	1.87
$\sigma(C4-C5)$	0.69	$\sigma^*(C7-C8)$	0.69	1.72
LP (1)O 3	1.73	$\pi^*(C3-C4)$	0.56	2.59
LP (2)O 3	0.69	$\sigma^*(N1-H6)$	0.73	4.32
LP(1) O4	1.55	$\sigma^*(N1-H7)$	0.77	2.43
LP(1) O4	0.75	$\sigma^*(N2-H8)$	0.72	3.81
$\sigma(O5-H11)$	2.21	$\sigma^*(N2-H9)$	0.72	1.65
$\sigma(O5-H12)$	1.16	$\sigma^*(N2-H10)$	0.72	1.89
$\sigma(O5-H12)$	1.26	$\sigma^*(C8-O4)$	0.75	2.65
LP(1) O5	0.33	$\pi^*(C8-O4)$	0.75	43.96
LP(2) O5	1.92	$\pi^*(C7-C8)$	0.52	50.68
LP(2) O5	1.87	$\pi^*(C2-C3)$	0.05	14.11
$\sigma(N2-H6)$	1.39	$\sigma^*(C8-O3)$	0.01	46.71
$\sigma(O4-C8)$	1.87	$\sigma^*(O5-H12)$	0.70	5.71
$\pi(O4-C8)$	0.92	$\sigma^*(O5-H11)$	0.69	7.35
$\pi^*(C4-C5)$	0.28	$\sigma^*(O1-H1)$	0.70	25.16
$\pi^*(C4-C5)$	0.28	$\sigma^*(O3-H11)$	0.69	37.31
$\pi(O2-C1)$	0.94	$\sigma^*(N2-H8)$	0.72	5.08
LP(2) O 2	0.66	$\sigma^*(N1-H7)$	0.96	13.44

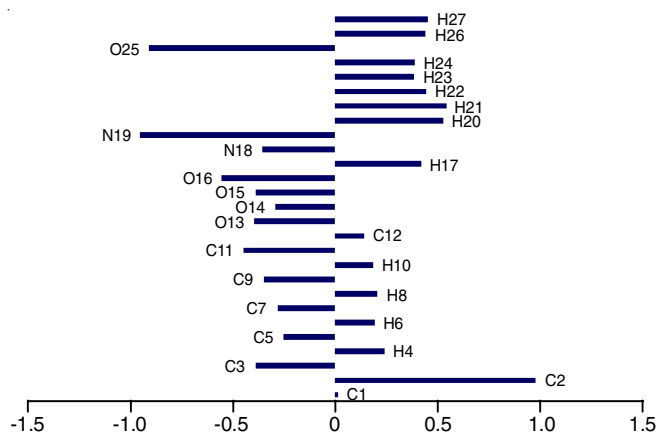


Fig. 6. Mulliken atomic charges plot of HHPMH

bonding. All the carbon atoms of phenyl ring show negative charge, except for C2 (0.9750 e). The C2 is attached to the carboxylic group.

Molecular electrostatic potential (MEP): Molecular electrostatic potential (MEP) affords very good information on the molecular regions that promote the electrophilic or nucleophilic attacks. It is widely applied in analyzing various biological systems for structure-property relations [25,26]. The negative MEP corresponds to nucleophilic sites (electron-rich center) shown as red shades on the MEP surface. Similarly, the

positive MEP corresponds to the electrophilic sites (electron-deficient center) shown as blue shades. Green shades indicate the neutral sites.

To predict the active sites for nucleophilic and electrophilic attacks [27] for the HHPMH, the electrostatic potential was calculated at the B3LYP/6-311G+ (d,p) level of basis set. The potential increases in the order red < orange < yellow < green < blue. The electrostatic potential diagram (Fig. 7) of the salt reveals that HHPMH exhibits positive potential on N₁₈-H and N₁₉-H atoms of hydrazinium moiety. The negative potential is observed on oxygen atoms of carboxylate ion, carboxylic acid and water molecules.

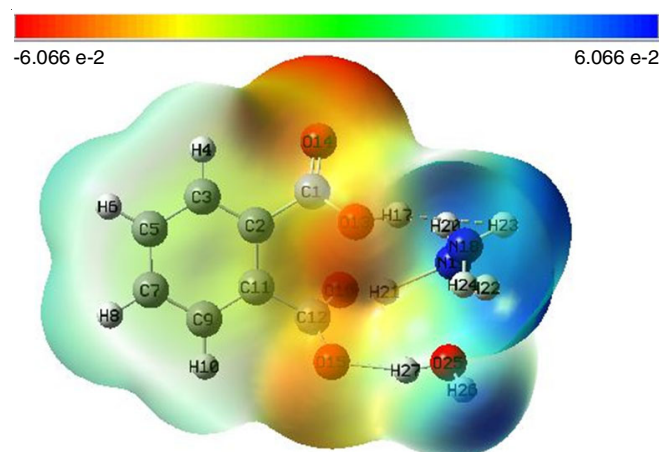


Fig. 7. Molecular electrostatic potential diagram of HHPMH

Frontier molecular analysis (FMO): The energy gap between the nearest bonding and antibonding orbitals (HOMO-LUMO) is an important factor, which decides the chemical reactivity and kinetic stability of the molecule. To explain the distribution of energy in the present ionic salt, the HOMO-LUMO energy calculations were carried out by B3LYP/6-311G+ (d,p) basis set. The electronic transition absorption corresponds to the transition from HOMO to the LUMO through electrons.

The HOMO is located and spread over both the carboxylate group and free carboxylic acid of the phthalic acid and hydrazine hydrate and LUMO is located and spread over on the one carboxylate group and hydrazinium ion (Fig. 8). The HOMO-LUMO energy gap is calculated as 7.7340 eV. This energy gap justifies the softness of the molecule which can be easily polarized and hence is more reactive.

Hirshfeld surface analysis: The Hirshfeld surface mapped with various properties, including shape index, d_{norm} and curvedness, was analyzed to understand the intermolecular interactions (Fig. 9). The surface of d_{norm} (d_e+d_i) shows intermolecular contact in relation to the radius of van der Waals with blue and red colour spots. The red spots represent strong hydrogen bonding and high electron density, whereas the blue spots indicate weak hydrogen bonding and lower electron density [28].

In Hirshfeld surface, curvedness is the measure of curvature. A small value of curvedness is associated with the flat surface area, whereas the areas with sharp curvature tend to classify a surface into patches associated with contact among neighbouring molecules and exhibit a large value of curvedness.

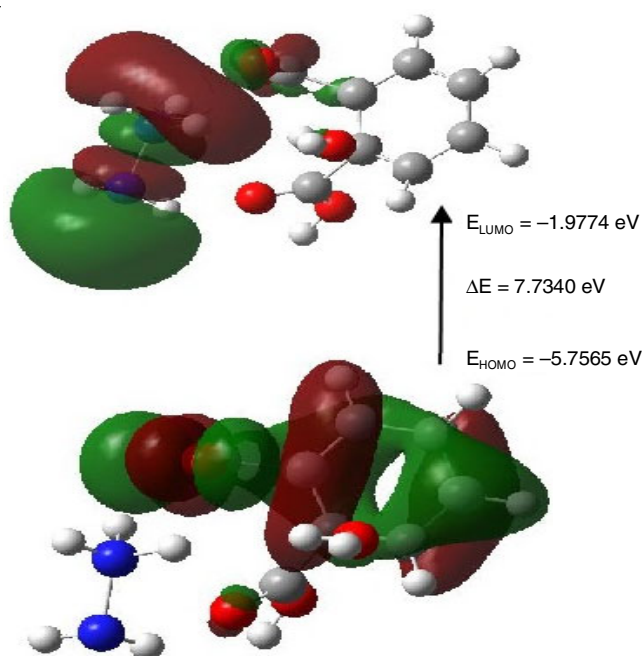


Fig. 8. Frontier molecular orbitals of HHPMH

Low curvedness represents close contact in the molecule probably caused by covalent bonding [29]. In the curved surface, the large flat region represented using the blue outline indicates the $\pi \cdots \pi$ stacking of molecules.

The shape index is used to determine the shape of the Hirshfeld surface. Red and blue triangles shown on the shape index indicate the concave regions representing the atoms of $\pi \cdots \pi$ stacking molecule above them and the convex regions denoting the ring atoms of the molecule inside these surfaces, respectively.

Fig. 10 presents the 2D fingerprint plots of the HHPMH crystal. In the 2D fingerprint plots, the portion of O \cdots H/H \cdots O interactions occupies (39%) of the overall Hirshfeld surface, with two unique spikes, which are the most crucial interactions in the crystal. Similarly, in the 2D plot, H \cdots H contact occupies a large area between the centres of the two large spikes; this large area contributes to 34.1% of the overall surface. Intramolecular N-H \cdots N interactions lead to 4.1% N \cdots H contact. Additionally, from the Hirshfeld surface analysis of HHPMH, reveals that the crystal exhibits other interatomic contact, including O \cdots O (1.9%) and C \cdots O (2.8%).

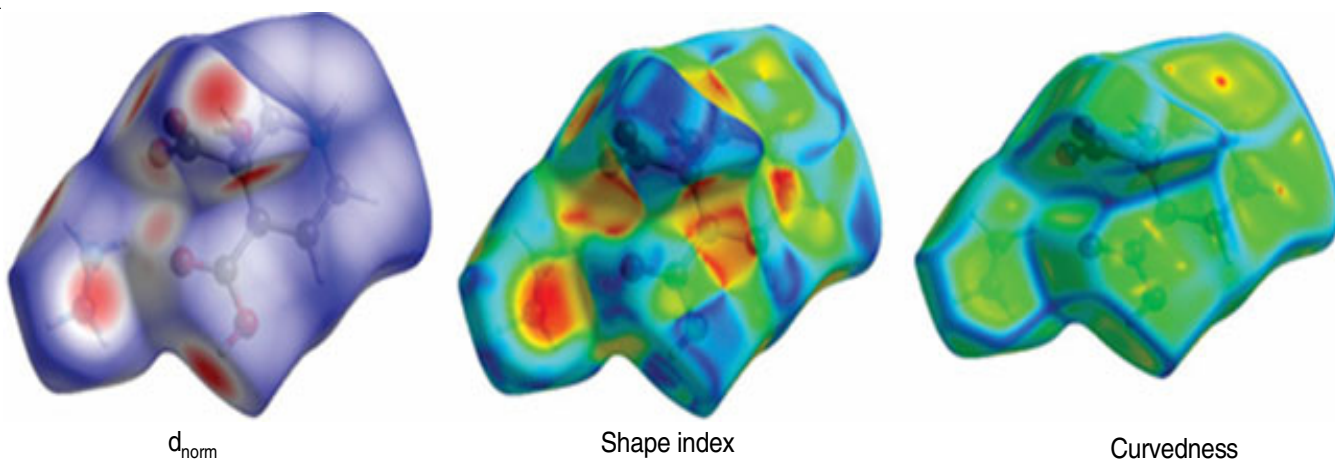
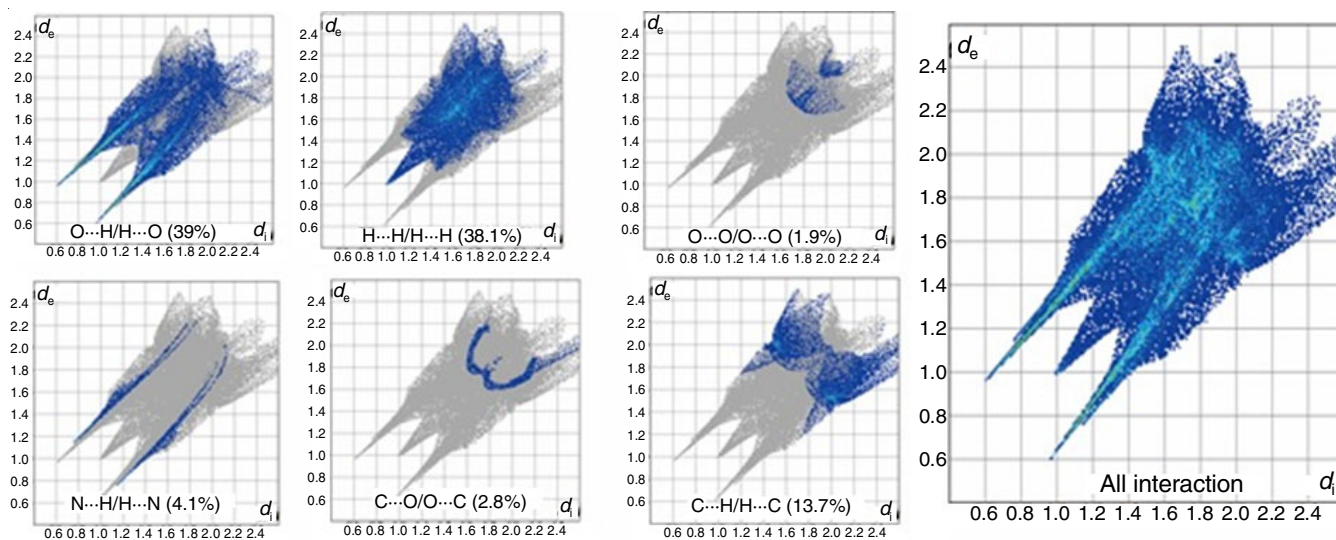
Fig. 9. Hirshfeld d_{norm} surface, Shape index, Curvedness of HHPM

Fig. 10. Hirshfeld 2D finger print plots of HHPMH

Conclusion

The pure single crystal of hydrazinium hydrogen phthalate monohydrate has been synthesized. Its formation was confirmed by analytical, spectral and X-ray single crystal studies. The nature of interactions between hydrazine cation and hydrogen phthalate anion were determined by Hirshfeld surface analysis. Thermal changes were monitored in the temperature range 0-850 °C and complete decomposition was confirmed. The molecular structure was optimized using B3LYP method by 6-311G (d,p) basis set. A theoretical calculation based on DFT and NBO analyses has been carried out to analyze molecular electrostatic potential. The optimized structure reveals that there is a good agreement with experimental observation.

ACKNOWLEDGEMENTS

One of the authors, (T.M. Ahamed Hussain) is grateful to University Grants Commission, New Delhi, India for RGNFD fellowship (Ref. No. F/2016-17/RGNFD-2016-17-TAM-2463).

CONFLICT OF INTEREST

The authors declare that there is no conflict of interests regarding the publication of this article.

REFERENCES

- B. Gu, C. Zhao, A. Baev, K.-T. Yong, S. Wen and P.N. Prasad, *Adv. Optics Photon.*, **8**, 328 (2016); <https://doi.org/10.1364/AOP.8.000328>
- D.R. Yuan, D. Xu, N. Zhang, M.G. Liu and M.H. Jiang, *Chin. Phys. Lett.*, **13**, 841 (1996); <https://doi.org/10.1088/0256-307X/13/11/011>
- I. Ledoux, *Synth. Met.*, **54**, 123 (1993); [https://doi.org/10.1016/0379-6779\(93\)91051-3](https://doi.org/10.1016/0379-6779(93)91051-3)
- H.A. Petrosyan, H.A. Karapetyan, M.Yu. Antipin and A.M. Petrosyan, *J. Cryst. Growth*, **275**, 1919 (2005); <https://doi.org/10.1016/j.jcrysgro.2004.11.258>
- H.O. Marcy, L.A. DeLoach, J.-H. Liao, M.G. Kanatzidis, S.P. Velsko, M.J. Rosker, L.F. Warren, C.A. Ebberts, P.H. Cunningham and C.A. Thomas, *Opt. Lett.*, **20**, 252 (1995); <https://doi.org/10.1364/OL.20.000252>
- D. Arivuoli, *PRAMANA-J. Phys.*, **57**, 871 (2001).
- S.S. Gupte, R.D. Pradhan, A. Marcano O, N. Melikechi and C.F. Desai, *J. Appl. Phys.*, **91**, 3125 (2002); <https://doi.org/10.1063/1.1436287>
- X. Liu, Z. Yang, D. Wang and H. Cao, *Crystals*, **6**, 158 (2016); <https://doi.org/10.3390/cryst6120158>
- F.A. Lopez, J.M. Cabrera and F.A. Rueda, *Electrooptics: Phenomena, Materials and Applications*, Academic Press: New York (1994).
- R. Hierle, J. Badan and J. Zyss, *J. Cryst. Growth*, **69**, 545 (1984); [https://doi.org/10.1016/0022-0248\(84\)90366-X](https://doi.org/10.1016/0022-0248(84)90366-X)
- A. Migalska-Zalas, K. El-Korchi and T. Chtouki, *Opt. Quant. Electron.*, **50**, 389 (2018); <https://doi.org/10.1007/s11082-018-1659-x>
- R. Rytel, G.F. Lipscomb, M. Stiller, J. Thackara and A.J. Ticknor, Eds.: J. Messier, F. Kajzar, P. Prasad and D. Ulrich, *Nonlinear Optical Effects in Organic Polymers*, Kluwer Academic Publishers, Dordrecht pp. 277-289 (1988).
- P. Muthuraja, T. Shanmugavadivu, T. Joselin Beaula, V. Bena Jothy and M. Dhandapani, *Chem. Phys. Lett.*, **691**, 114 (2018); <https://doi.org/10.1016/j.cplett.2017.11.003>
- P. Dhamodharan, K. Sathya and M. Dhandapani, *Physica B*, **508**, 33 (2017); <https://doi.org/10.1016/j.physb.2016.12.009>
- A. Dhandapani, S. Manivarman and S. Subashchandrabose, *Chem. Phys. Lett.*, **655-656**, 17 (2016); <https://doi.org/10.1016/j.cplett.2016.04.009>
- B.N. Sivasankar and S. Govindarajan, *Synth. React. Inorg. Met.-Org. Chem.*, **25**, 31 (1995); <https://doi.org/10.1080/15533179508218200>
- S.A. Hady, I. Nahringsbauer and I. Olovsson, *Acta Chim. Scand.*, **23**, 2764 (1969); <https://doi.org/10.3891/acta.chem.scand.23-2764>
- C. Sonia and B.N. Sivasankar, *Synth. React. Inorg. Met.-Org. Chem.*, **44**, 1119 (2014); <https://doi.org/10.1080/15533174.2013.799195>
- K. Kuppusamy, B.N. Sivasankar and S. Govindarajan, *Thermochim. Acta*, **259**, 251 (1995); [https://doi.org/10.1016/0040-6031\(95\)02257-3](https://doi.org/10.1016/0040-6031(95)02257-3)
- A. I. Vogel's, *A Textbook of Quantitative Inorganic Analysis*, Longmans: London, Ed.: 3 (1962).
- C.K. Johnson, ORTEP ORNL-3794, Oak Ridge National Laboratory, Tennessee (1976).
- G.M. Sheldrick, *SHELXL-2014 Programs for Crystal Structure Determination*, University of Cambridge, England (2015).
- S.K. Wolff, D.J. Grimwood, J.J. McKinnon, M.J. Turner, D. Jayatilaka and M.A. Spackman, *Crystal Explorer (Version 17.1)*, University of Western Australia (2017)
- M.J. Frisch, G.W. Trucks, H.B. Schlegel, G.E. Scuseria, M.A. Robb, J.R. Cheeseman, G. Scalmani, V. Barone, G.A. Petersson, H. Nakatsuji, X. Li, M. Caricato, A.V. Marenich, J. Bloino, B.G. Janesko, R. Gomperts, B. Mennucci, H.P. Hratchian, J.V. Ortiz, A.F. Izmaylov, J.L. Sonnenberg, D. Williams-Young, F. Ding, F. Lipparini, F. Egidi, J. Goings, B. Peng, A. Petrone, T. Henderson, D. Ranasinghe, V.G. Zakrzewski, J. Gao, N. Rega, G. Zheng, W. Liang, M. Hada, M. Ehara, K. Toyota, R. Fukuda, J. Hasegawa, M. Ishida, T. Nakajima, Y. Honda, O. Kitao, H. Nakai, T. Vreven, K. Throssell, J. A. Montgomery, Jr., J.E. Peralta, F. Ogliaro, M.J. Bearpark, J.J. Heyd, E.N. Brothers, K.N. Kudin, V.N. Staroverov, T.A. Keith, R. Kobayashi, J. Normand, K. Raghavachari, A.P. Rendell, J.C. Burant, S.S. Iyengar, J. Tomasi, M.J.M. Cossi, M. Klene, C. Adamo, R. Cammi, J.W. Ochterski, R.L. Martin, K. Morokuma, O. Farkas, J.B. Foresman and D.J. Fox, *Gaussian 16, Revision B.01*, Gaussian, Inc., Wallingford CT (2016).
- P. Politzer, P.R. Laurence and K. Jayasuriya, *Environ. Health prospect*, **61**, 191 (1985); <https://doi.org/10.1289/ehp.8561191>
- J. Lu, W.R. Kobertz and C. Deutsch, *J. Mol. Biol.*, **371**, 1378 (2007); <https://doi.org/10.1016/j.jmb.2007.06.038>
- T. Karthick and P. Tandon, *J. Mol. Model.*, **22**, 142 (2016); <https://doi.org/10.1007/s00894-016-3015-z>
- L. Skovsen, M. Christensen, H.F. Clausen, J. Overgaard, C. Stiewe, T. Desgupta, E. Mueller, M.A. Spackman and B.B. Iversen, *Inorg. Chem.*, **49**, 9343 (2010); <https://doi.org/10.1021/ic100990a>
- J.J. McKinnon, D. Jayatilaka and M.A. Spackman, *Chem. Commun.*, 3814 (2007); <https://doi.org/10.1039/b704980c>